

Neutral pressure measurement in TCV tokamak using ASDEX-type pressure gauges

G. Sun¹, H. Reimerdes, H. Elaian, M. Baquero-Ruiz, M. Gospodarczyk, M. Noël, E. Tonello, and the TCV team²

Ecole Polytechnique Fédérale de Lausanne (EPFL), Swiss Plasma Center (SPC), CH-1015 Lausanne, Switzerland

Probing the neutral gas distribution at the edge of magnetic confinement fusion devices is critical for divertor physics studies. In the TCV tokamak, a set of ASDEX-type hot ionization pressure gauges (APGs) has been installed for fast, in-situ measurements of the neutral pressure distribution in the TCV chamber. The APGs have been calibrated against baratron pressure gauges (BGs) for pressures ranging from less than 1 mPa to several hundred mPa. A correction to account for the residual pressure in the pumped torus is proposed to improve the measurement accuracy. APG measurements in a series of plasma discharges with varied density ramp rates are analyzed, and are compared with the pressure measurements of the existing BGs. APG measurements feature significantly higher time resolution and faster time response than the BGs, and extend the measurement range to lower pressures. APGs systematically measure higher neutral pressures than the BGs connected to the same TCV port, likely due to the BG time delay and slow time response and nonuniform neutral distribution in gauge ports during the discharge. The initial APG operations in TCV have been proven successful, which validates the APG as an adequate pressure measurement technique for the upcoming TCV divertor upgrades.

I. INTRODUCTION

Neutral particles play an essential role in the operation of magnetic confinement fusion devices. Common physical quantities used to characterize the neutral distribution in fusion devices are the divertor neutral pressure, $P_{n,div}$, and the neutral compression, c_n , which is the ratio of divertor to main chamber neutral pressures. High values of $P_{n,div}$ or c_n generally favor the access to a detached divertor, an operation mode widely assumed to be necessary in future fusion reactors for tolerable power exhaust. A linear parameter dependence of $P_{n,div}$ for pronounced a detachment condition was observed in AUG tokamak [1]. Additionally, $P_{n,div}$ is related to the upstream separatrix density [2], which is limited by the global density limit [3]. In

¹ Author to whom any correspondence should be addressed.

² See H. Reimerdes et al 2022 Nucl. Fusion 62 042018 for the TCV team.

TCV, different shapes of neutral gas baffles have been installed, aiming for better divertor neutral confinement, i.e. higher $P_{n,div}$ and c_n for the same upstream conditions [4]. Precise and accurate measurements of these neutral-related quantities are hence crucial to validate the effectiveness of the gas baffles.

The neutral pressure used to be only measured with BGs in TCV [5]. However, these BGs suffer from a considerable time delay and a slow time response, as they are connected to the TCV chamber via long extension tubes (of the order of two meters). Furthermore, the BGs cannot resolve pressure levels below several mPa, expected in the main chamber of the baffled TCV divertor [6]. These limitations have motivated the installation ASDEX-type pressure gauges (APGs), which were specifically designed for in-situ, fast measurement of the neutral pressure in wide pressure ranges for magnetic confinement fusion devices [7].

APGs are a type of hot ionization gauge designed for high magnetic field and noisy environments, which were originally developed by G. Haas and first deployed in ASDEX [7, 8]. APGs have been installed in a range of tokamaks and stellarators, including AUG [9], DIIIID [10], EAST [11], KSTAR [12], ADITYA [13], LHD [14], W7-X [15] and are foreseen for ITER [16]. However, the APG operation in fusion devices is subject to a range of technical challenges. The gauge filament, usually made of tungsten, is exposed to strong, cyclical $J \times B$ forces and thermal stresses, which may cause creep and fatigue of the filament [17]. Additionally, APG measurement can suffer from small current jumps [18], and are affected by impurity neutrals [19] and time-varying magnetic field during the measurement [20]. All these concerns must be addressed to ensure long-term, stable APG operation in fusion devices. The present work introduces the APG setup, highlights the issues that were encountered and proposes improvements that should be implemented, before employing APGs in the next TCV upgrade.

This article is structured as follows. Section II recaps the working principle of APG and introduces the APG setup in TCV. Section III provides the detailed procedure employed to calibrate TCV's APGs. Section IV compares the APG and BG measurement in TCV plasma discharges with varied density ramp rates. Concluding remarks are given in section V.

II. Diagnostic setup

This section briefly reviews the working principle of APG (see [7] for more details) before presenting their setup in TCV, including the gauge head design, remote control, automation, and integration of the diagnostic into the TCV discharge cycle.

A. Working principle of the ASDEX-type pressure gauge

The APG is a hot-cathode ionization pressure gauge [21], optimized for applications under strong magnetic field. The APG head consists of a filament, a control electrode (CE), an acceleration grid (AG), and an ion collector (IC), which are linearly aligned along the magnetic field on an electrically insulated base plate, Figure 1(a). The filament is a thoriated tungsten wire biased at 70 V, and is heated to emit thermionic electrons by a DC current of typically 20 A to achieve the reference electron current of 200 μ A. The filament is usually shaped with two symmetrical “single spirals”, which has been proved optimized for the mechanical stability. [17, 22]. The CE is a metal plate featuring a wide slit perpendicular to the magnetic field and parallel to the base plate, whose potential varies between 0 and 120 V to chop the collected current signals at a frequency of 5 kHz. The AG is also a metallic plate with an even wider slit that contains an acceleration grid, biased at 250 V. The IC is a simple metal plate biased at the filament potential of 70 V.

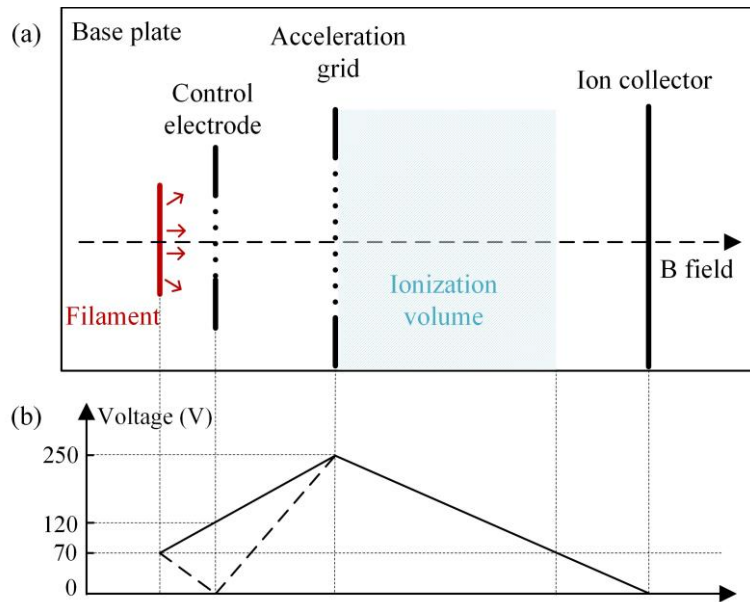


Figure 1. (a) Schematic top view of the APG head. Dotted lines in the control electrode and the acceleration grid are the slits. (b) The electrode biased voltages and the voltage distribution with dashed lines representing the voltage distribution during the control electrode chopping.

Electrons emitted from the heated filament are confined by the space potential between the filament and the IC, where they oscillate with kinetic energies sufficient to ionize neutrals, Figure 1(b). The ion current resulting from electron-impact ionizations in the ionization volume, and electron current, are collected at the IC and AG, respectively. The neutral density in the ionization volume, Figure 1(a), can then be determined from the two measured currents.

The ion current collected at the IC, I^+ , depends on the neutral density in the ionization volume, and the electron current. The electron current, I^- , depends on the total emitted electron flux at the filament and AG’s transparency and is collected at the AG. The sensitivity, d , of most types of ionization gauge is conventionally defined as:

$$d = \frac{I^+}{(I^- - I^+)n_g}, \quad (1)$$

with n_g being the neutral density in the ionization volume. Denominator of Equation (2) is a correction at high neutral densities where I^+ is comparable with I^- , which removes the electron current due to secondary electrons generated from the ionizations.

A more physical expression for APG's sensitivity can be derived by calculating the ionization rate induced by oscillating electrons in the ionization volume at given potential distribution shown in Figure 1 (see Equations (1)-(10) in [7]):

$$d = \frac{2 \int_0^{e(U_{AG} - U_{Fil})} \sigma_{ion} d\varepsilon \cdot x_{max} [1 + S(f-1)]}{e(U_{AG} - U_{Fil}) \left[\frac{1-\theta}{\theta} + S \right]} \quad (2)$$

Here θ is the transparency of the AG, S is the surviving probability, f is electron oscillation number, x_{max} is the size of the ionization volume, U_{AG} and U_{Fil} are voltages of AG and the filament, and σ_{ion} is the electron-impact ionization cross section of the gas in the ionization volume. Clearly, the sensitivity depends on the gas species, and the APG measurement in deuterium plasmas is affected by the presence of impurity neutrals, e.g. discharges with impurity seeding. The gauge sensitivity is determined by in-situ gauge calibrations. Though the sensitivity should be independent of the neutral density according to Equation (2), section III will show that this is not always observed in practice, and corrections are needed.

With the gauge measuring the neutral density inside the gauge head, further considerations are needed to link this density to the neutral pressure in the vicinity of the gauge head. Note that the APG head is shielded by a stainless steel cube with a small entrance hole to reduce the neutral conductance between the ionization volume and the region around the gauge. This ensures that neutral particles inside the gauge undergo many wall collisions and thermalize with the gauge head temperature. The neutral distribution outside the gauge is not necessarily at the same temperature as the gauge head, nor even a Maxwellian distribution. Since in stationary conditions, the influx of neutral particles through the gauge head hole matches the outflux of thermalized particles, the APG measurement can be interpreted as a measurement of the neutral flux towards the entrance hole. This interpretation requires the knowledge of the gas temperature inside the gauge head, which is assumed to be at room temperature. An increase of gas temperature in the gauge head due to filament heating was verified to be negligible, by monitoring the gas temperature of gauge head during an extended filament heating period than the 10 s in experiment, using a thermal imaging camera.

B. APG setup in TCV

The APGs are designed to routinely operate during TCV discharges. The diagnostic is, hence, automated and integrated into the general TCV discharge cycle, to minimize the need for manual actions by the diagnostic operator. The current APG setup in TCV is introduced below.

The APG diagnostic system in TCV consists of a National Instrument chassis (NI-PXIe-8821) containing the embedded Windows PC with LabVIEW installed and an FPGA card. The FPGA card is programmed to execute the overall control of the APG measurement. It is connected to four gauge controllers (NGas modules³), which provide bias voltages to the filament, AG and CE, and measures the currents to AG and IC. The NGas modules are each connected to a filament power supply (TDK-Lambda, GEN20-38) for filament heating, and to the gauge head where the measurement is performed⁴, Figure 2(a). The NGas module, FPGA code and the LabVIEW program were provided by IPP-Garching. The current setup with four NGas modules allows simultaneous operation of up to four APGs. The gauges are located in a port at the top (labeled ‘top’), the high-field side floor (labeled ‘div’), the low-field side floor (labeled ‘bot’), and at the outer mid-plane (OMP) (labeled ‘mic’) of the TCV chamber, Figure 2(b). In typical lower-single null configurations the ‘div’ and ‘bot’ gauges measure the pressure in the private- and common-flux-regions of the divertor, respectively. The gauges ‘div’, ‘bot’, and ‘mic’ are installed in ports that also connect to corresponding BGs to facilitate the gauge commissioning. NGas modules and filament power supplies, both, are controlled remotely. The filament power supplies are switched on for entire days with TCV operation, while the NGas modules are only switched on for each TCV discharge when human access to the tokamak is prohibited, due to the high bias voltages.

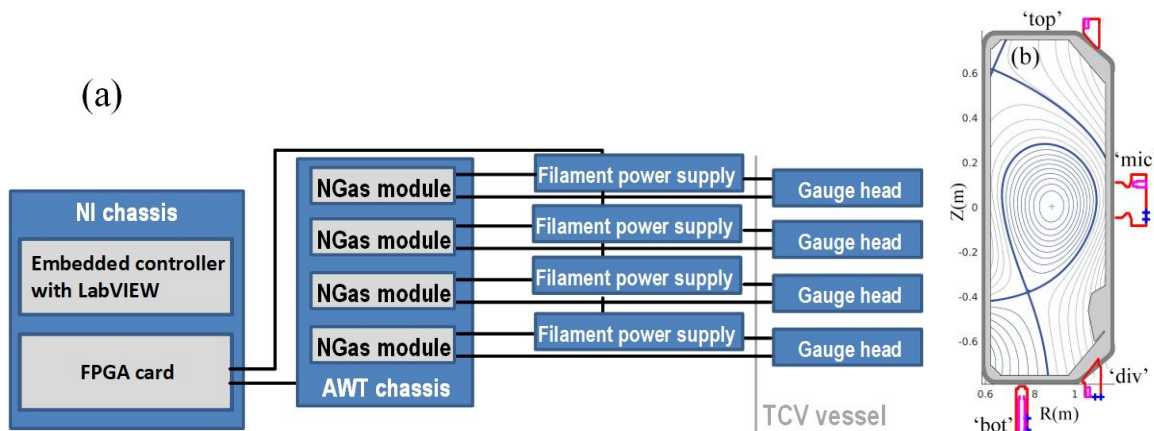


Figure 2. (a) Schematic of the APG measurement system in TCV. (b) Locations of the APG and BG ports. The red contours are port structures containing the gauge heads, the magenta contours are the APG heads, and the blue points are opening for the tubes connected to the BGs.

³ The NGas modules were purchased from Arbeitsgruppe Weltraumphysik und–technologie (AWT).

⁴ The gauge heads were purchased from IPT-Albrecht GmbH.

The entire gauge head is shielded from the tokamak environment by a stainless steel cube featuring a small entrance hole, which is covered by a curved metallic sheet, to allow gas flow into the gauge head while protecting against fast neutrals, Figure 3. The leads of the gauge are covered by metallic circular tube to shield the signal cables against the potential influence of radiation on the current measurements, which is most obvious at the outer mid-plane gauge position, Figure 3.

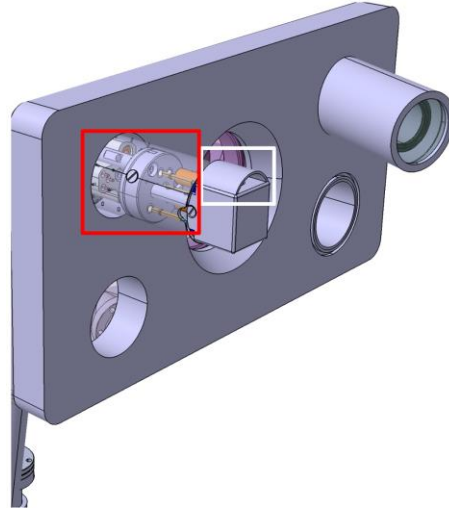


Figure 3. CAD image of the mid-plane gauges with the curled metallic sheet above the entrance hole (marked by white box), and the circular tube covering the leads of the gauge head (marked by red box).

Before operation starts, the communication between the filament power supply, NI controller and the FPGA must first be established, and remains active during the entire experimental session. The electron current collected on the AG, I^- , is maintained at a reference level (generally $200 \mu\text{A}$) by a PID controller, which adjusts the filament heating current during the APG operation. The APG measurement is triggered seven seconds before the discharge starts, to leave sufficient time to establish the requested value of I^- . Depending on the estimated neutral pressure at the gauge locations, an appropriate ion current gain is selected for each gauge prior to each measurement. After each TCV discharge, measured electron and ion currents are saved in MDS nodes of the TCV database. The neutral density and the corresponding neutral pressure are calculated according to Equation (1), using sensitivities that are determined in calibrations, section III.

III. Calibration of the APG diagnostic

The sensitivity, Equation (1), is not a priori known and must be determined in a calibration. The sensitivity depends on the filament geometry, implicitly included in the surviving probability S in Equation (2) [7]. As a result, recalibration of the gauges is necessary if the filament is severely deformed by the $\mathbf{J} \times \mathbf{B}$ force.

The APG sensitivities are determined by cross-calibrating with BGs, using the duration of gas flow to extend the BG pressure range to lower values. The various steps of an APG calibration in TCV are described as follows.

A. Design of the calibration pulses

The gauge sensitivity can be determined by performing a scan of neutral pressure values, and calculating the sensitivity at each neutral pressure level from the measured of I^+ and I^- , using Equation (2). This procedure motivates the design of APG calibration pulses in TCV.

The APG calibration pulses feature the typical toroidal field of 1.43 T of a TCV plasma discharge, but no poloidal fields and transformer currents. The gate valves of TCV's four turbo-molecular pumps are closed before deuterium gas (D_2) is injected into the vessel via a piezo valve. The neutral pressure distribution in TCV chamber then quickly becomes uniform.⁵

D_2 is injected in three short pulses, typically separated by 0.6 s, leading to three discrete increases of the D_2 pressure and four measurement intervals with constant pressure, Figure 4(a). The duration of a calibration pulse is limited by the toroidal field coil power supplies. The first pressure measurement interval starts at $t = -0.05$ s, when magnetic field reaches 1.43 T. The subsequent measurement intervals start 0.4 s after each D_2 pulse yielding interval durations of 0.2 s, where the measured quantities including currents and pressures are assumed constant and averaged, Figure 4(b). The delay between gas pulses and measurement intervals is determined by the time response of the BGs. APG calibration in TCV typically covers a pressure range from 0.5 mPa to over 200 mPa.

⁵ The injected gas expands from the gas valve to the TCV chamber. The characteristic time of gas expansion in TCV chamber is estimated from $t_{expand} \sim \frac{\pi R}{v_{D_2,th}}$, which is approximately 2 ms. Here R is the major radius and $v_{D_2,th}$ the thermal velocity of deuterium molecules at room temperature.

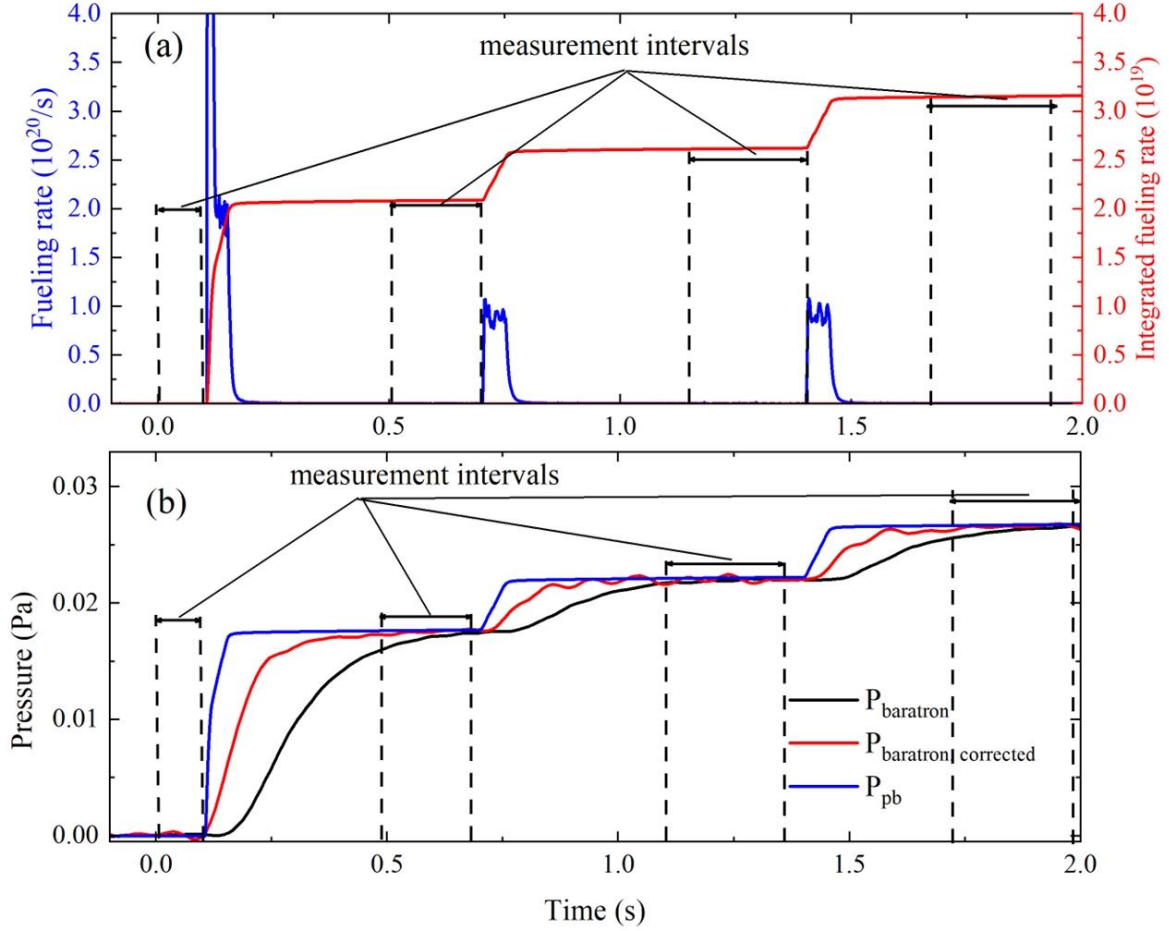


Figure 4. (a) Deuterium fueling rate (left axis) and its integral over time (right axis) of TCV calibration pulse #77961. (b) Original BG pressure, corrected BG pressure (see section IIIB), and pressure based on particle balance assuming a TCV volume of 4.86 m^3 , of TCV calibration pulse #77961. The four measurement intervals are marked. The magnetic field reaches 1.43 T at $t = -0.05 \text{ s}$ and remains constant until 2 s .

B. Pressure estimation based on the particle balance

Since APGs seek to extend the measurement range below the BG limit, a direct cross-calibration with the BGs is not sufficient. This difficulty is resolved by estimating the neutral pressure from the gas valve fluxes, based on the neutral particle balance.

The particle-balance estimate of the neutral pressure P_{pb} is obtained from the integrated deuterium fueling rate:

$$P_{pb} = \frac{k_B T_g}{V_{TCV}} \int \Gamma_D dt, \quad (3)$$

where k_B is the Boltzmann constant, T_g is the gas temperature (300 K), V_{TCV} is TCV vessel volume and Γ_D is the deuterium fueling rate. The value of V_{TCV} is determined by comparing the integrated Γ_D with BG pressures within the BG range of measurement.

Furthermore, the BGs suffer from a time delay and a slow time response that can be corrected by deconvolving the system response with the following transfer function:

$$h(t) = \frac{1}{\tau_{resp}} \exp\left(-\frac{t-\tau_{delay}}{\tau_{resp}}\right) u(t - \tau_{delay}), \quad (4)$$

and the following relation for signal convolution:

$$P_{baratron,measured}(t) = P_{baratron,real}(t) * u(t) \quad (5)$$

Here the function u is the Heaviside step function, $P_{baratron,real}$ is the real pressure measured by the BGs (the pressure obtained by performing the deconvolution), and $P_{baratron,measured}$ is the pressure measured by BG. The response time $\tau_{resp} \approx 0.10s$ and delay time $\tau_{delay} \approx 0.04s$ are determined from TCV discharges. The correction can effectively remove the effects of finite BG time response and time delay on the measurement, Figure 4(b).

By assuming that the corrected BG pressure is equal to particle balance estimate of pressure in each measurement interval, a linear fit based on Equation (3) yields an estimate of $V_{TCV} = 4.86 \text{ m}^3$.

C. Treatment of the ion current offset

The determination of the APG sensitivity requires an accurate ion current signal. The ion current is expected to be approximately proportional to the neutral pressure, Equation (1), whereas potential offsets introduce systematic errors, in particular at low pressures. A separation of measured offsets into contributions from the residual pressure in the pumped vessel and noise reduces this systematic error.

The ion current offset has a non-negligible influence on the measurement at low neutral pressure (below 1 mPa) where the offset is comparable to the ion current signal. The evolution of the ion current before the first gas pulse has three phases, Figure 5. A nonzero ion current offset exists from the beginning of measurement even before the electron current emerges at approximately $t = -3 \text{ s}$ (phase 1). From $t = -3 \text{ s}$ to -1.2 s , the ion current slightly increases and saturates with the electron current at a higher value, but before applying the magnetic field (phase 2). The ion current further increases after the magnetic field is applied (phase 3). The phase 1 offset is independent of the ion current gain. The phase 2 offset depends on the electron current, and phase 3 depends on both electron current and the magnetic field.

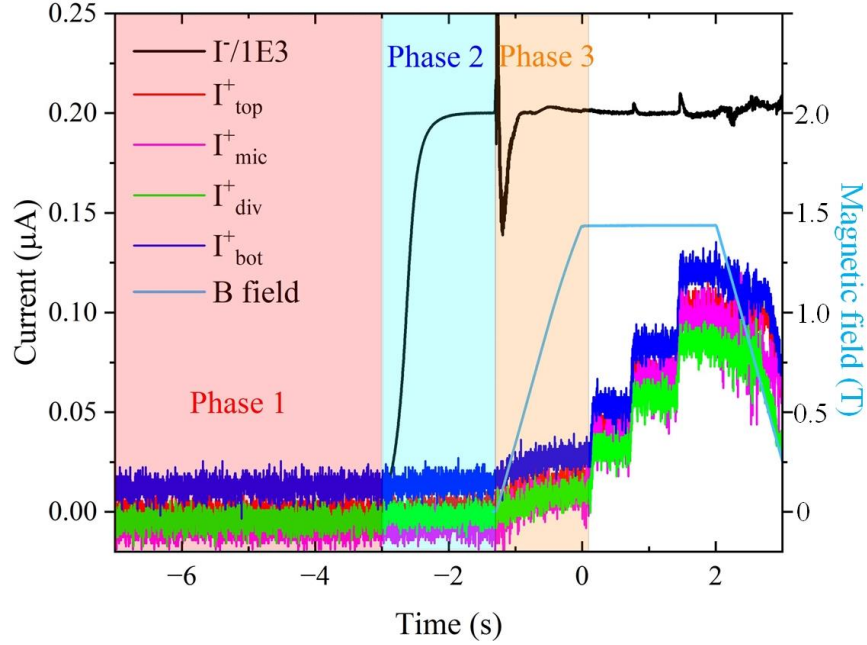


Figure 5. Normalized electron current of the APG ‘mic’, ion currents of four gauges, and the magnetic field of a low-pressure calibration pulse #77960, to better visualize the evolution of current offsets. The electron current is maintained at 200 μA during the measurement and the magnetic field ramps up to 1.43 T before descending. Ion current offsets in phase 1-3 are marked in shaded areas.

The phase 1 offset exists even without electron current, hence without electrons that may ionize any neutrals and is, therefore, linked to the circuit noise. The increments of the offsets in phase 2 and 3 are likely caused by a residual pressure before the gas injection. Note, that the BG signal is set to zero just before gas is injected into the torus. Therefore, the residual pressure is excluded in the BG measurement. In phase 2, the electron current can already lead to the ionization of any residual gas and hence increases the ion current offset even if the electrons are not confined by a magnetic field. The phase 3 offset exceeds the phase 2 offset (both corrected for the phase 1 offset), by approximately one order of magnitude. This increase is presumably caused by the increase of the electron confinement in the direction perpendicular to the electric field by the magnetic field. In Equation (2), this increase of confinement is reflected by an increase of the electron oscillation number f . The increase of ion current with magnetic field is supported by tests of an APG in a vacuum chamber, where the effect of magnetic field saturates when field is higher than approximately 1.0 T, consistent with previous observations [7]. The phase 1 ion current offset is, therefore, subtracted when analyzing the calibration pulses and I^+ will henceforward refer to the offset corrected ion current measurement.

D. Residual pressure correction

The phase 2 and 3 ion current offsets discussed in section III C suggest a significant residual pressure, $P_{residual}$, before the deuterium injection in the calibration pulses, and should be added to the gas-balance pressure:

$$\frac{I^+}{I^- - I^+} = \frac{d}{k_B T_g} (P_{pb} + P_{residual}) \quad (6)$$

The value of $P_{residual}$ is obtained for each calibration pulse by fitting the measurement of I^+ and P_{pb} of the four measurement intervals to Equation (6), Figure 6. The values of $P_g^{residual}$ of the four gauges obtained in a calibration pulse are similar, but vary among calibration pulses. The residual pressure is generally below 0.5 mPa, and is likely related to the duration of the time interval between closing the gate valve and separating the turbo pumps from the TCV vessel. The residual pressures of four APGs are averaged for a calibration pulse, and the total pressure $P_{tot} = P_{pb} + \overline{P_{residual}}$ of each measurement interval will be used for the sensitivity calculation in section III E.

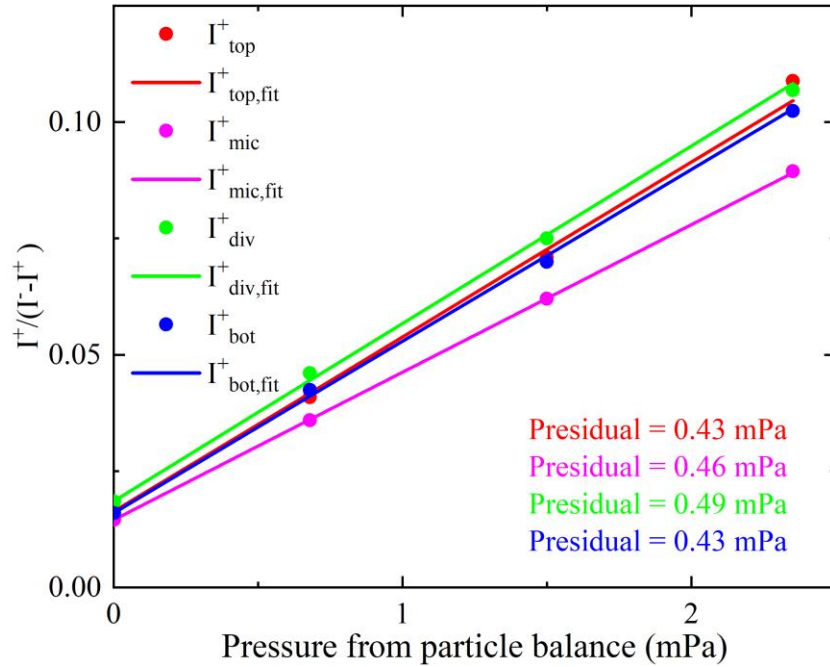


Figure 6. The averaged $\frac{I^+}{I^- - I^+}$ and P_{pb} of the four measurement intervals of the calibration pulse #77960 for four APGs, and the linear fits to determine the residual pressure based on Equation (6).

E. Calculation of the sensitivity at reference electron current

The sensitivities of each measurement interval in all calibration pulses are obtained using Equation (6). The residual pressure correction leads to a sensitivity that varies little with pressure, Figure 7.

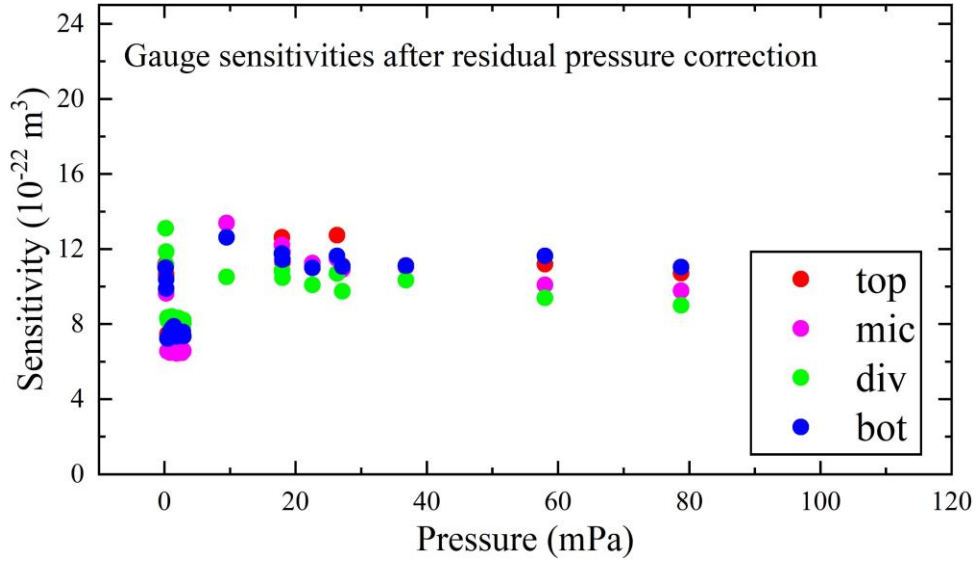


Figure 7. The dependency of gauge sensitivity on neutral pressure with the residual pressure correction, of the calibration session in August, 2023.

F. Sensitivity with varying electron current

The calibration procedure introduced above determines the gauge sensitivity at an electron current of 200 μA , which is typically used in TCV discharges. In APG operations, fluctuations of I^- are frequently observed when the plasma conditions evolve quickly, such that the I^- value may deviate from the reference level while the controller adjusts the filament heating current. To improve the measurement precision during such I^- fluctuations, the reference electron current is varied, and the obtained sensitivities, Figure 8, are parameterized with two parameters d_0 and A , following [7]:

$$d = d_0 \left(\frac{A}{I^-} + 1 \right) \quad (7)$$

The pressure measured by an APG is then calculated as:

$$P_{APG} = \frac{I^+}{I^- - I^+} \frac{k_B T_g}{d_0 \left(\frac{A}{I^-} + 1 \right)} \quad (8)$$

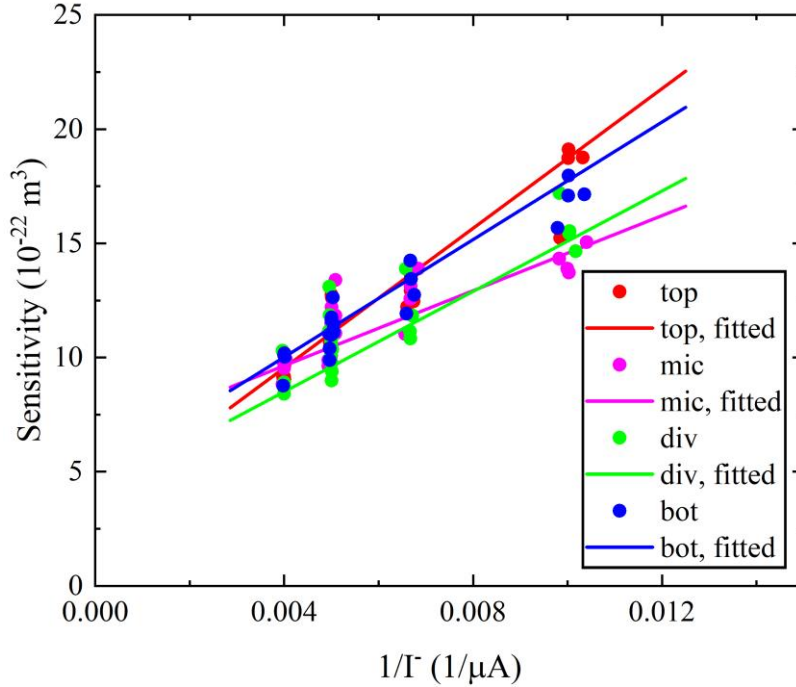


Figure 8. Dependency of the sensitivities of the TCV gauges on the reciprocal of the electron current.

IV. Evaluation of the APG performance

The performance of the APGs in TCV is evaluated in comparison with the BGs, both in the calibration pulses without plasma, and in TCV plasma discharges. The advantages of APGs are described and causes of the pressure measurement discrepancies are analyzed.

A. Comparison of APG and BG measurements in TCV calibration pulses

The APG-measured pressure, calculated from the sensitivities determined in section III, is compared with the BG-measured pressure for two representative APG calibration discharges at low-pressure and high-pressure levels, Figure 9. The APG measurement features a clear residual pressure, and responds quickly to D_2 injection with negligible time delay and a fast time response, Figure 9(a). The APG measurement in the low-pressure discharge confirms that the APG can resolve pressures as low as 0.5 mPa. The BG pressure, both original and the corrected, can hardly resolve the first two pressure measurement intervals. The BG pressure also exhibits strong irregular signal oscillations, amplified by the deconvolution procedure, which are observed at low-pressure levels.

The APG-pressure rises with the gas injection with a time delay (τ_{delay}) of approximately 3 ms, which is one order of magnitude lower than the delay of the BG. The APG time delay likely due to the combination of molecule time of flight (approximately 2 ms) and averaging over chopping intervals (0.2 ms). The APG also features a response time of 0.02 s, which

is one fifth of the BG response time. Therefore, APG features much faster time response than the BG, which is also shown in the high-pressure calibration pulse, where the APG pressures reach the constant level in a measurement interval after a D_2 pulse faster than the BG corrected for τ_{delay} , Figure 9(b).

The APG signal features a signal oscillation of less than 0.5 mPa, visible in Figure 9(a), which does not vary significantly with the pressure, Figure 9(b). The APG pressure, however, exhibits “pressure jumps” in the third and fourth pressure measurement intervals of the high-pressure calibration pulse, where the measured pressure repetitively switches between two fixed levels during a measurement interval, suggesting transition between two or more modes. Such jump also appears for the ion current, which has been also observed during APG operations in W7-X and AUG [18, 23]. Recent studies proposed that the ion current jump is likely related to the two-stream instabilities due to electron oscillations, a counter-streaming motion, between the filament and the ion collector [18]. Dedicated simulations of the APG plasma are needed to validate this hypothesis and seek potential mitigation approaches of the ion current jump. Though the ion current jump may jeopardize the accuracy of the diagnostic, it is not corrected for the moment due to limited understanding of its underlying mechanisms.

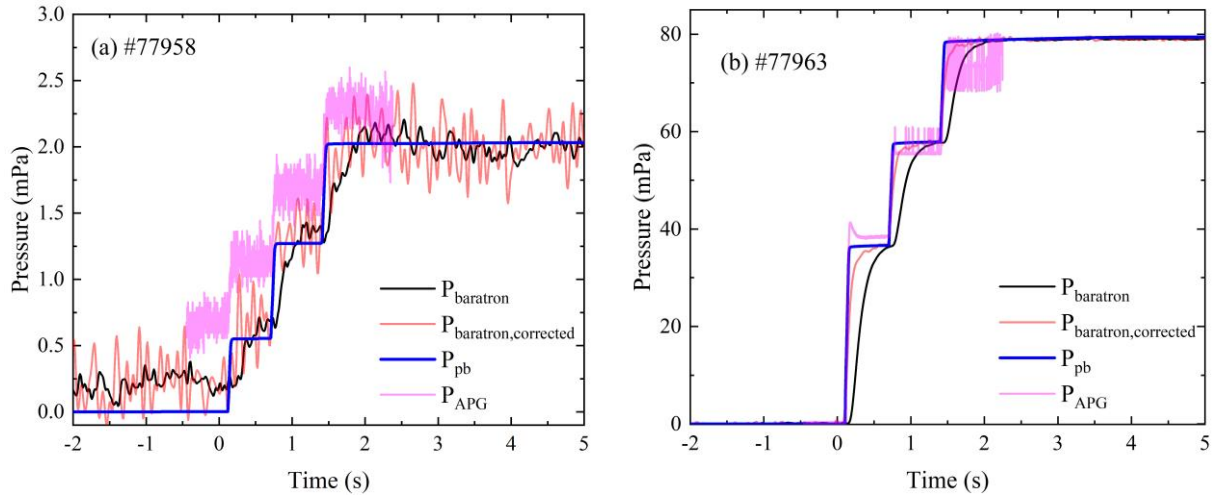


Figure 9. Original BG pressure, corrected BG pressure, pressure based on particle balance, and the APG pressure of the TCV calibration pulse #77958 and #77963. Only outer mid-plane gauges are compared.

B. Comparison of APG and BG measurements in TCV plasma discharges

To evaluate the APG performance in TCV plasma discharges, the pressures measured in a series of Ohmic density ramp discharges by three APGs (‘div’, ‘bot’, and ‘mic’) are compared with the pressure measured by the BGs installed in the same ports, Figure 10. The selected discharges have a plasma current of 250 kA and were performed in TCV’s short inner, long outer (SI-LO) baffle configuration.

Prior to a TCV plasma discharges, the vessel is filled with deuterium gas starting at $t = -0.1$ s. The gas break down is induced through the application of a large loop-voltage at approximately $t = 0$ s. The shown discharge disrupts at $t = 1.1$ s. During the entire discharge, the APG measurements feature a faster time response and a lower time delay than the BGs, as in the non-plasma pulses in Figure 9. While APG and BG measurements generally agree before and after the plasma discharge, i.e. when the vessel is primarily filled with deuterium gas, the APG-measured pressures are systematically higher in the presence of plasma in the vessel. The difference is clearly visible on the divertor gauges, Figure 10(a), (b), whereas in the outer mid-plane, the BG cannot resolve the pressure very well as the neutral pressure during plasma discharge is below 5 mPa, Figure 10(c). The BG measurement exhibits strong oscillations while the APG can resolve the mid-plane pressure below 5 mPa. During the density ramp, the corrected BG pressures in the divertor CFR and PFR are higher than the BG pressure during the discharge, due to the slower time response and considerable time delay of BGs [thesis, CC]. However, the correction for BG measurement alone cannot fully explain the discrepancy between APG and BG measurements.

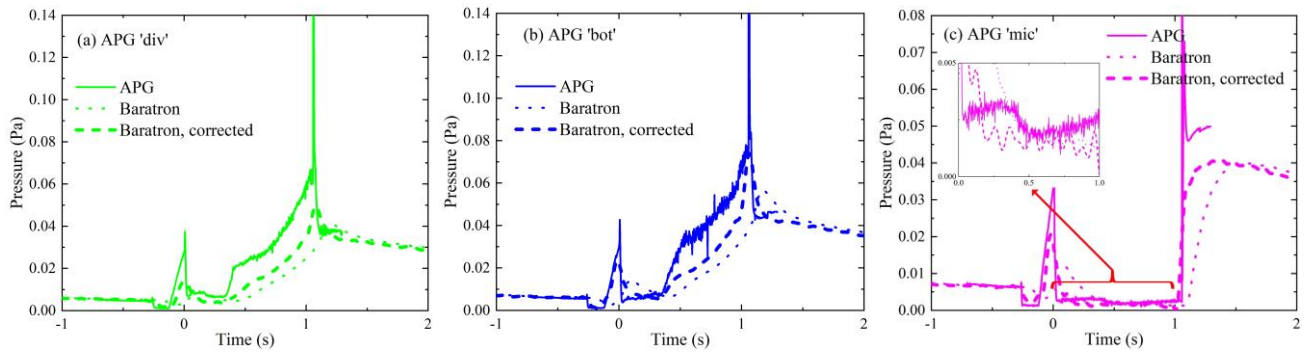


Figure 10. Example of the APG, original and corrected BG measurements for a TCV discharge with a density ramp (#78188). The APGs and BGs are located at the same ports of (a) the divertor 45 degree tile (common flux region), 'div', (b) private flux region, 'bot', and (c) the outer mid-plane, 'mic'. The insert in (c) highlights the measurements between $t = 0$ s and 1 s.

A comparison of the APG and BG measurements in several TCV discharges with different density ramp rates shows the extent of the disagreement, Figure 11. In the presence of plasma, the APG systematically measures a pressure that is approximately 70% higher than the BG pressure. The pressure levels at the outer mid-plane is low and is beyond the BG measurement limit, hence the mid-plane BG pressure is scattered and no clear pressure dependence on the APG pressure is found.

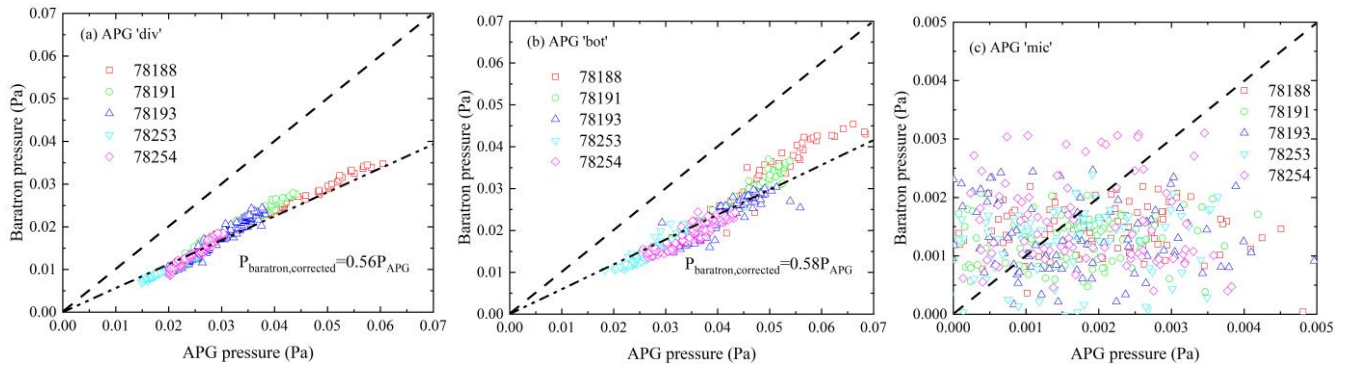


Figure 11. Comparison of APG and corrected BG measurements at the same TCV ports. (a) Divertor 45 degree tile (common flux region). (b) Divertor private flux region. (c) Outer mid-plane. Five discharges with density ramp rate increasing from $3.5 \text{ m}^{-3}\text{s}^{-1}$ to $7.8 \text{ m}^{-3}\text{s}^{-1}$ are selected for the comparison.

C. Analysis of the pressure measurement discrepancies

The remaining discrepancies between APG and BG measurements can have several reasons. A key observation is that the discrepancies in the measured pressures only occur when the torus is filled with plasma, and the neutrals in the vicinity of the gauge are only partially recombined to molecules, with atoms having a non-Maxwellian distribution. One possible explanation is that the neutral distribution in the gauge ports is nonuniform during the discharge.

To validate this hypothesis, SOLPS ITER 3.0.8 code package is used to model the deuterium neutral distribution during a plasma discharge in the TCV gauge ports. The SOLPS-ITER code couples the 2D fluid transport code B2.5 and the 3D kinetic neutral transport code EIRENE [24]. The code employs axisymmetric geometry, including axisymmetric gauge port structures, and can, therefore, only provide a qualitative assessment. The employed magnetic equilibrium corresponds to the configurations used in the density ramp experiments described in Section IVB. Considered plasma species are deuterium and carbon, and the deuterium is fueled from the outer divertor common flux region. The simulation setup such as the boundary conditions, considered reactions, and transport coefficients, corresponds to previous work using the same magnetic equilibrium [25]. The adopted magnetic equilibrium, plasma and neutral grid, and gauge locations are shown in Figure 12. The extended gauge port structures at the top, the high-field side floor, the low-field side floor, and the outer mid-plane of the TCV chamber are based on realistic TCV port geometry but are axisymmetric due to code limitations.

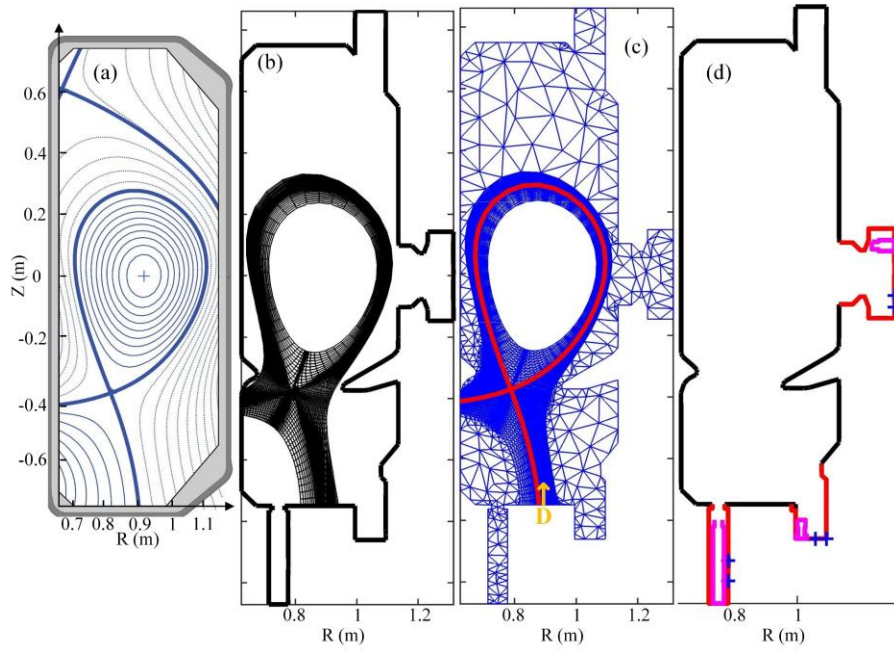


Figure 12. (a) Employed TCV magnetic equilibrium. (b) B2.5 grid (c) EIRENE grid, where the deuterium fueling location is marked by an arrow. (d) Locations of the APG probe head (magenta) and the openings for the BG extension tubes (blue).

Synthetic pressure measurements are obtained from SOLPS-ITER simulations based on a 0D neutral transport model which translates the fluxes of neutral atoms and molecules and $\Gamma_{D,edge}$ to the pressure measured with the gauges:

$$P_{Syn,gauge} = k_B \sqrt{T_{wall}} (\Gamma_{D,edge} + \Gamma_{D_2,edge}) \quad (9)$$

T_{wall} is the wall temperature and is assumed to be 300 K. The model assumes molecular flow, neutral flux conservation, and full recombination and thermalization of atomic deuterium due to wall collisions. The model has been validated for the BGs in previous work by analytical calculation and SOLPS-ITER simulation of the BG extension tube, where the neutral collision mean free path is proved to be much smaller than the BG extension tube diameter, and the neutrals are fully thermalized at the end of the extension tube [26]. Equation (9) is used to calculate synthetic APG and BG measurements by averaging neutral flux on the surface elements near the APG heads, and the surface elements at the openings for BG extension tubes, respectively.

The neutral pressures from synthetic APG measurement exceeds the synthetic BG measurement in the divertor and outer mid-plane by 40%, 45%, 66%, respectively, Table 1.

Table 1. Synthetic pressure measurement from SOLPS

Pressure (mPa)	bot	div	mic
APG	10.3	15.0	0.5
BG	7.4	10.3	0.3

The synthetic pressure values suggest that the neutral distribution can be nonuniform in the gauge ports. SOLPS-ITER simulations predict that neutral density in the gauge port is lower near the port entrance, and increases away from the port entrance, particularly in corner regions without direct line of sight facing the SOL plasma, Figure 13. Note that the neutral density and energy both affect the neutral flux into the gauge, so that the relative importance of values in Table 1 is not always reflected in Figure 13.

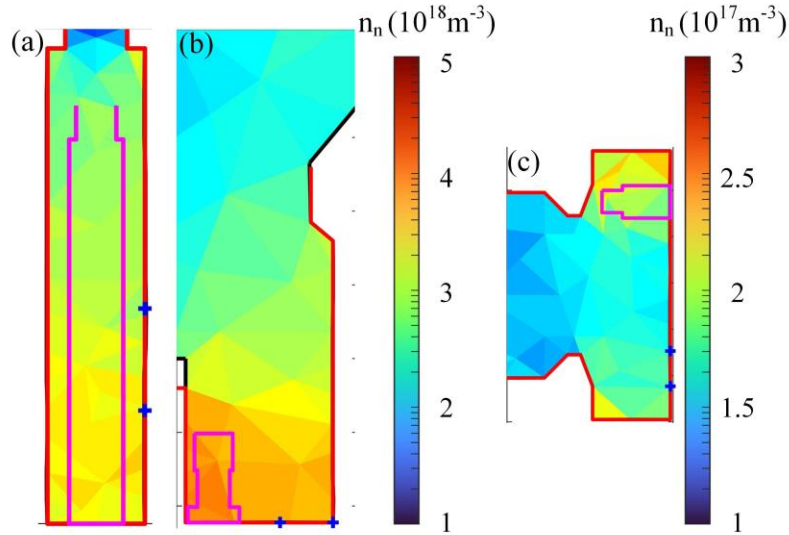


Figure 13. Neutral deuterium density distribution in the three gauge ports predicted by SOLPS-ITER simulation. (a) APG ‘bot’. (b) APG ‘div’. (c) APG ‘mic’. The magenta structures are transport to the neutrals and are added only to evaluate the neutral fluxes in the simulated volume. The blue crosses mark the entrance to the BG extension tubes.

The SOLPS-ITER simulation reproduce the direction and the order of magnitude of the difference between particle fluxes into the APGs and BGs needed to explain the apparent discrepancies. A quantitative comparison would require a realistic 3D port geometry and a precise description of the divertor plasma in the simulation.

In conclusion, the APGs installed in TCV exhibit significantly faster time response and lower time delay than the TCV BGs. There are discrepancies between the BG and APG measurement, due to two reasons: (1) BGs have slower time response and larger time delay than the APG. (2) Neutral pressure distribution is nonuniform in the gauge port during plasma discharge. Further investigations are expected in future APG operations in TCV to better interpret the two types of pressure measurement.

V. Conclusion

ASDEX-type pressure gauges have recently been installed in the TCV tokamak to measure the neutral pressure distribution at the top, the high-field side floor, the low-field side floor, and the outer mid-plane of the TCV vessel. The APGs were fully

integrated into the TCV discharge cycle. The APGs are calibrated for D_2 using calibration pulses. The pressure is estimated from the gas injection rate and the neutral particle balance based on a cross calibration with baratron gauges at sufficiently high pressures. Measured ion current must be corrected for an offset due to electronic noise and the estimated residual pressure that is present before the programmed gas flow. Sensitivities are determined at different pressure and electron current levels. The calibration procedure yields sensitivities which do not greatly vary with the neutral pressure and vary linearly with the reciprocal of electron current. The performances of the APGs and the BGs located at the same TCV ports are compared, showing much faster time response, lower time delay, and much better pressure resolution in low-pressure ranges below 5 mPa of the APGs. The discrepancy between APG and BG measurement can be explained by differences in the time delay and time response, and a nonuniform neutral distribution in the gauge ports during the TCV discharge. The initial APG operations in TCV are promising, and validate that APGs should be reliable for pressure measurement in the next TCV upgrade.

Acknowledgments

This work has been carried out within the framework of the EUROfusion Consortium, via the Euratom Research and Training Programme (Grant Agreement No. 101052200— EUROfusion) and funded by the Swiss State Secretariat for Education, Research and Innovation (SERI). Views and opinions expressed are however those of the author(s) only and do not necessarily reflect those of the European Union, the European Commission, or SERI. Neither the European Union nor the European Commission nor SERI can be held responsible for them. This work was supported in part by the Swiss National Science Foundation. The authors would like to thank Dr. Felix Mackel, Dr. Michael Griener from Max-Planck Institute for Plasma Physics, and Mr. Wolfgang Noack from Arbeitsgruppe Weltraumphysik und-technologie for helpful discussions and continued support.

References

- [1] Kallenbach A, Bernert M, Beurskens M, Casali L, Dunne M, Eich T, Giannone L, Herrmann A, Maraschek M, Potzel S, Reimold F, Rohde V, Schweinzer J, Viezzer E, Wischmeier M and the A U T 2015 Partial detachment of high power discharges in ASDEX Upgrade *Nuclear Fusion* **55** 053026
- [2] Kallenbach A, Bernert M, Dux R, Eich T, Henderson S S, Pütterich T, Reimold F, Rohde V and Sun H J 2019 Neutral pressure and separatrix density related models for seed impurity divertor radiation in ASDEX Upgrade *Nuclear Materials and Energy* **18** 166-74

- [3] Martin G 2002 Density limits in toroidal plasmas *Plasma Physics and Controlled Fusion* **44** R27
- [4] Reimerdes H, Duval B P, Elaian H, Fasoli A, Février O, Theiler C, Bagnato F, Baquero-Ruiz M, Blanchard P, Brida D, Colandrea C, De Oliveira H, Galassi D, Gorno S, Henderson S, Komm M, Linehan B, Martinelli L, Maurizio R, Moret J M, Perek A, Raj H, Sheikh U, Testa D, Toussaint M, Tsui C K, Wensing M, Tcv team t and Eurofusion Mst1 team t 2021 Initial TCV operation with a baffled divertor *Nuclear Fusion* **61** 024002
- [5] Theiler C, Lipschultz B, Harrison J, Labit B, Reimerdes H, Tsui C, Vijvers W A J, Boedo J A, Duval B P, Elmore S, Innocente P, Kruezi U, Lunt T, Maurizio R, Nespoli F, Sheikh U, Thornton A J, van Limpt S H M, Verhaegh K, Vianello N, the T C V t and the E M S T t 2017 Results from recent detachment experiments in alternative divertor configurations on TCV *Nuclear Fusion* **57** 072008
- [6] Reimerdes H, Alberti S, Blanchard P, Bruzzone P, Chavan R, Coda S, Duval B P, Fasoli A, Labit B, Lipschultz B, Lunt T, Martin Y, Moret J M, Sheikh U, Sudki B, Testa D, Theiler C, Toussaint M, Uglietti D, Vianello N and Wischmeier M 2017 TCV divertor upgrade for alternative magnetic configurations *Nuclear Materials and Energy* **12** 1106-11
- [7] Haas G and Bosch H S 1998 In vessel pressure measurement in nuclear fusion experiments with asdex gauges *Vacuum* **51** 39-46
- [8] Team A, Haas G, Gernhardt J, Keilhacker M and Meservey E B 1984 Measurements on the particle balance in diverted ASDEX discharges *Journal of Nuclear Materials* **121** 151-6
- [9] Zito A, Wischmeier M, Kappatou A, Kallenbach A, Sciortino F, Rohde V, Schmid K, Hinson E T, Schmitz O, Cavedon M, McDermott R M, Dux R, Griener M, Stroth U and the A U T 2023 Investigation of helium exhaust dynamics at the ASDEX Upgrade tokamak with full-tungsten wall *Nuclear Fusion* **63** 096027
- [10] Shafer M W, Covele B, Canik J M, Casali L, Guo H Y, Leonard A W, Lore J D, McLean A G, Moser A L, Stangeby P C, Taussig D, Wang H Q and Watkins J G 2019 Dependence of neutral pressure on detachment in the small angle slot divertor at DIII-D *Nuclear Materials and Energy* **19** 487-92
- [11] Zhou D, Yu Y, Wang C, Cao B, Zuo G and Hu J 2023 Measurement of divertor neutral pressure in EAST tokamak by ASDEX pressure gauge *Fusion Engineering and Design* **196** 114024
- [12] Kim M, Kim K and Lee H 2019 The new attempts for the in-vessel pressure gauge operation in the KSTAR plasma *Fusion Engineering and Design* **146** 2011-4
- [13] Patel K, Jadeja K A, Joshi H C and Ghosh J 2019 The data acquisition and control system for the operation of ASDEX pressure gauge for the measurement of neutral pressure in ADITYA Tokamak *Fusion Engineering and Design* **148** 111256
- [14] Haak V, Motojima G, Jagielski B, Naujoks D, Graband A and Pilopp D 2024 Performance of LaB₆-Emitters for Neutral Gas Pressure Gauges During Plasma Operation in the Large Helical Device *IEEE Transactions on Plasma Science* 1-5
- [15] Haak V, Bozhenkov S A, Feng Y, Kharwandikar A, Kremeyer T, Naujoks D, Perseo V, Schlisio G, Wenzel U and the W X T 2023 Overview over the neutral gas pressures in Wendelstein 7-X during divertor operation under boronized wall conditions *Plasma Physics and Controlled Fusion* **65** 055024
- [16] Mackel F, Arkhipov A, Asad W, Meister H, Valente P and Andrew P 2023 Testing of ITER diagnostic pressure gauges in preparation of final design review *Fusion Engineering and Design* **189** 113439

- [17] Arkhipov A, Mackel F, Haas G, Koll J, Meister H, Seyvet F, Terron S and Andrew P 2020 Mechanical Stability of Filaments for ITER Diagnostic Pressure Gauges Relating to Creep and Fatigue *IEEE Transactions on Plasma Science* **48** 1661-5
- [18] Castillo A C, Mackel F, Griener M, Birkenmeier G and Team t A U 2022 Experimental investigation of current jumps in linear geometry hot cathode ionization gauges in strong magnetic fields *Fusion Engineering and Design* **181** 113194
- [19] Ichimura K, Yamashita S and Nakashima Y 2019 Study on the sensitivity of fast ionization gauge in mixture gas of hydrogen and helium *Plasma and Fusion Research* **14** 34051241-5
- [20] Silva R A S, Bundaleski N and Teodoro O M N D 2022 Effect of the magnetic field on the operation of ionisation gauges *Vacuum* **204** 111339
- [21] Jousten K, Boineau F, Bundaleski N, Illgen C, Setina J, Teodoro O M N D, Vicar M and Wüest M 2020 A review on hot cathode ionisation gauges with focus on a suitable design for measurement accuracy and stability *Vacuum* **179** 109545
- [22] Arkhipov A, Mackel F, Haas G, Koll J, Scarabosio A, Meister H, Seyvet F, Terron S and Andrew P 2018 Experimental validation of thermo-mechanical simulations of ITER diagnostic pressure gauges *Fusion Engineering and Design* **136** 398-402
- [23] Wenzel U, Schlisio G, Mulsow M, Pedersen T S, Singer M, Marquardt M, Pilopp D and Rüter N 2019 Performance of new crystal cathode pressure gauges for long-pulse operation in the Wendelstein 7-X stellarator *Review of Scientific Instruments* **90**
- [24] Wiesen S, Reiter D, Kotov V, Baelmans M, Dekeyser W, Kukushkin A S, Lisgo S W, Pitts R A, Rozhansky V, Saibene G, Veselova I and Voskoboynikov S 2015 The new SOLPS-ITER code package *Journal of Nuclear Materials* **463** 480-4
- [25] Sun G, Reimerdes H, Theiler C, Duval B P, Carpita M, Colandrea C, Février O and the T C V T 2023 Performance assessment of a tightly baffled, long-legged divertor configuration in TCV with SOLPS-ITER *Nuclear Fusion* **63** 096011
- [26] Wensing M, Duval B P, Février O, Fil A, Galassi D, Havlickova E, Perek A, Reimerdes H, Theiler C, Verhaegh K, Wischmeier M, the E M S T t and the T C V t 2019 SOLPS-ITER simulations of the TCV divertor upgrade *Plasma Physics and Controlled Fusion* **61** 085029